Supplement to "Exploring drift simulations from ocean circulation experiments: application to cod eggs and larval drift"

Arne Melsom Kristina Øie Kvile Knut-Frode Dagestad
Göran Broström Øystein Langangen

S1. Regional decomposition

In order to compile statistics and analysis results in geographical regions, a subdivision of the R4 domain has been defined. This subdivision is presented in Fig. S1, and region names are given in the figure legend. An important aspect in the definitions of the regions is that the large scale cyclonic circulation in the Nordic Seas follow lines of constant bottom depth (Jakobsen et al. 2003), with latitudinal contrasts due to the regional seasonal signal. The following are the main criteria applied in order to separate regions:

- The 800 m isobath has been used to separate coastal regions 1,2,4-6,8-10,12,14,17 from the deep basin to the west (to the north for regions 1,2)
- The Norwegian Trench (region 2) is defined as the region in the North Sea were the bottom depth exceeds 250 m.
- Vestfjorden (region 7) has been introduced in order to make tracer seeding regions

Vestfjorden and *Yttersida* belong to different analysis regions (seeding regions are introduced in section 2.4).

- The Vøring Plateau (region 21) is a geographical feature with depths $<$1500 m extending from the continental shelf into the Norwegian Sea
- The Lofoten Basin (region 20) is defined as the deep ocean which in the north is limited by the 2500 m isobath (depths $>$2500 m are displayed by the darkest shade of blue in Fig. 1.)

A set of larger subdivisions achieved by merging selections of the regions, are also considered extensively in the analysis. These subdivision are introduced in order to study how properties evolve geographically along the Norwegian coast (region 3-9), in the Barents Sea (10-14), and in the Norwegian Sea deep basin (region 18-22).

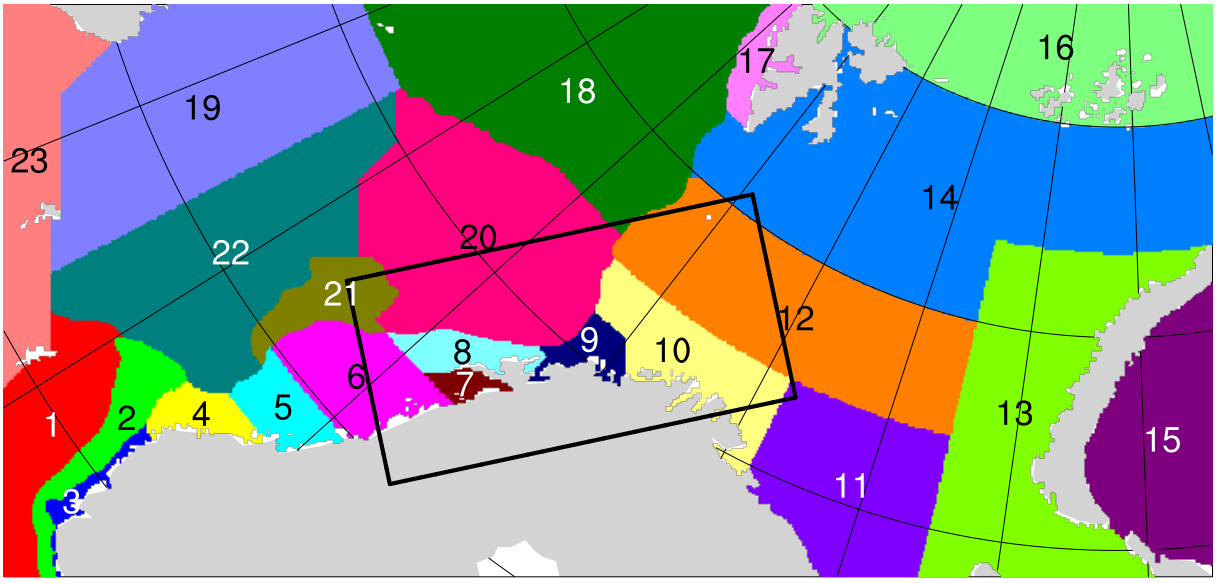

Fig. S1. The 23 analysis regions defined in the 4km model configuration: (1) North Sea, (2) Norwegian Trench, (3) North Sea coast, (4) Møre coast, (5) Trønderlag coast, (6) Helgeland coast, (7) Vestfjorden, (8) Lofoten/Vesterålen, (9) Troms coast N, (10) Barents Sea SW, (11) Barents Sea SE, (12) Barents Sea central, (13) Barents Sea E, (14) Barents Sea N, (15) Kara Sea, (16) Arctic Ocean, (17) Svalbard W, (18) Norwegian Sea N, (19) Norwegian Sea W, (20) Lofoten Basin, (21) Vøring Plateau, (22) Norwegian Sea SE, (23) Shetland-Faeroe Islands-Iceland. See the text for details.

S2. Application of lift velocity

In order to shed light on how a lift velocity affects the tracer results, we digress from the ROMS experiments for a moment. Here, we apply a much simpler one dimensional model that solves the diffusion equation (Fick 1855) in the absence of fluid motion. Denote the tracer concentration and the vertical lift velocity by c and w_0, respectively. Furthermore, denote a constant diffusion coefficient by κ. Finally, let h_e and h_i be the exponential decay of the initial distribution and the depth below which the initial distribution is set to 0, respectively. With conditions of a vanishing gradient at infinite depth and conservation of the initial tracer mass, the steady state solution becomes

$$c(z) = \frac{h_e}{h_0}[1 - e^{-h_i/h_e}]e^{z/h_0} \quad , \quad h_0 = \frac{\kappa}{w_0} \tag{S1}$$

and an approximation for the level of the gravity center, z_g, reveals the following relation:

$$z_g = \int_{-\infty}^{0} zc(z)dz \Big/ \int_{-\infty}^{0} c(z)dz \qquad \Rightarrow \qquad \kappa = -z_g w_0 \tag{S2}$$

In all experiments a lift velocity $w_0 = 0.0013$ m/s (110 m/day) was applied to the tracers. As explained in section 2.4, we arrived at this value from shorter test experiments for tracers. By inspecting the simulation results in Fig. 2b, we find that the vertical center of gravity for tracer concentration is approximately in the range 8-12 m. Using the simple diffusion model outlined above, a gravity center at 10 m will then result when the mixing coefficient is set to $\kappa = 0.013$ m^2/s, due to relationship in equation S2.

The resulting vertical distributions after 12 hours and the steady state are shown in Fig. S2 by the blue and red full lines, respectively. Also displayed with dashed lines are results for the case with no vertical lift and a vanishing tracer gradient at a bottom depth of 200 m. We note that in this simple one dimensional model a lift velocity can

be introduced to counter the tendency towards a uniform distribution so that the initial center of gravity is nearly stationary. Obviously, without a lift the center of gravity moves towards the halfway point between the surface and the bottom.

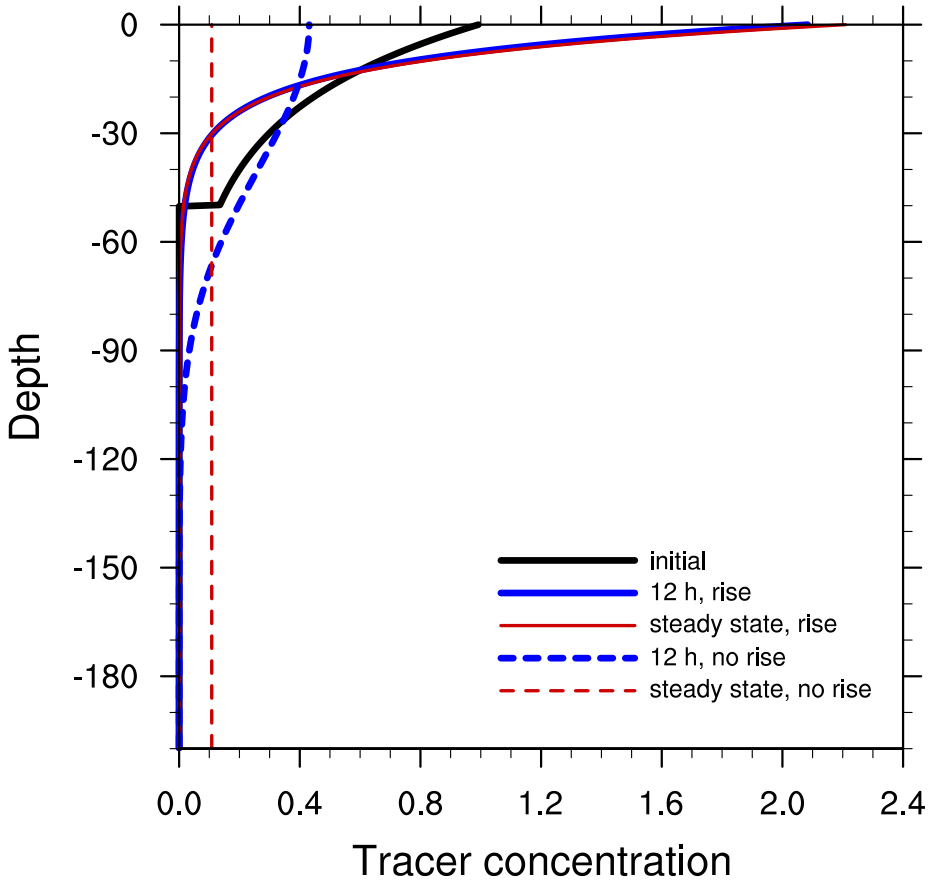

Fig. S2. Effect of introducing a lift velocity to a diffusive tracer. The initial vertical distribution profile (black line) is the same as the initial condition for tracers in the ocean circulation model experiments. Solid lines corresponds to results obtained when a rise velocity of 0.0013 m/s is applied. Dashed lines show the profiles when only diffusive processes act on the tracer. Here, we have prescribed a vertical eddy diffusivity coefficient of 0.013 m^2/s.

Unfortunately, results for vertical velocity were not stored from the ROMS simulations, but results for vertical mixing (turbulent kinetic energy and turbulent generic length scale) were available. Hence, particle advection in the *OpenDrift* simulations was computed from horizontal velocities from the experiment results, supplemented by vertical

motion as derived from the parameterization of vertical mixing in *OpenDrift*'s *OpenDrift3D* module. This configuration for vertical motion is similar to the implementation of vertical tracer mixing. Hence, the same lift velocity ($w_0 = 0.0013$ m/s) was applied.

S3. Trajectory filter

In order to effectively exclude the tidal motion from a trajectory we have adopted a simple box filter for intervals corresponding to two M_2 periods, which is 24.84 h. In the present analysis, results for online floats are recorded at an interval of $\Delta t = 1\,\mathrm{h}$. Denoting the trajectory position coordinates by (x^p, y^p), the filtered trajectory $(\overline{x^p}, \overline{y^p})$ at time t is then defined as

$$\overline{x^p}(t), \overline{y^p}(t) = \frac{\sum_{i=-12}^{12} w_i x^p(t + i\Delta t), y^p(t + i\Delta t)}{\sum_{i=-12}^{12} w_i} \ ,$$
$$w_{-12} = w_{12} = 0.92 \ ; \ \ w_j = 1, j = -11, \ldots, 11 \tag{S3}$$

A segment of a sample trajectory is displayed by a blue curve in Fig. S3, with the filtered trajectory in red.

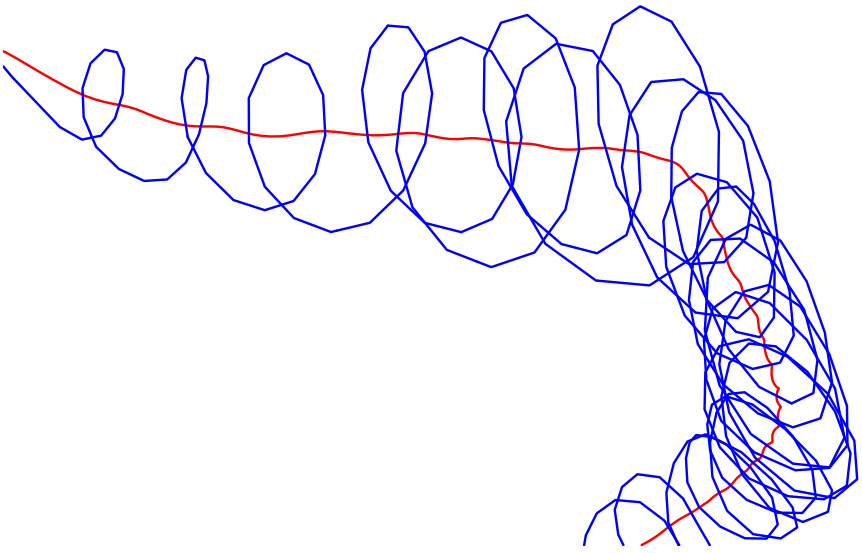

Fig. S3. Segment of sample trajectory. Illustrated here is the impact of applying the temporal filter to produce a box filtered trajectory. The distance from left to right in this figure is 20 km. The original trajectory recorded for an online float in an R0.8 simulation is is displayed as a blue curve, while the filtered trajectory is in red.

S4. Model validation

Model results for temperature and salinity are here compared with data from the World Ocean Database (Boyer et al. 2013). The total numbers of profiles in the domain covered by the 4 km resolution configuration (Fig. S1) are 4055 (1966), 6002 (1980), 3695 (1992), and 2623 (2006). Note that some profiles have temperature data only, while a smaller number have salinity data only. Model results for salinity and temperature were derived from profiles of the daily averages of the model results at the date of the available observations.

We present results for bias, anomaly correlation and a rank score, for temperature and salinity. This analysis is based on profile averages in the upper 100 m of the water column, consistent with the depth restriction for float trajectories which was introduced in section 3.1. The biases are computed by subtracting observational data (x^o) from the corresponding model results (x^m):

$$BIAS(r,y) = \frac{1}{N(r,y)} \sum_{n=1}^{N(r,y)} [x_n^m - x_n^o] \tag{S4}$$

where r is the analysis region, y is the observation year, and $N(r,y)$ are the number of observations in region r during year y. Thus bias values are aggregated in the 23 analysis regions defined in section S1, and the averages of these results for the four simulation years are displayed in Fig. S4a,b.

The salinity bias is positive along the coast of Norway, with large values in the south, and bias values in the range $0.1 - 0.5$ in analysis region 5 (Trøndelag coast) and northwards. The strong positive bias in the Norwegian coast combined region is a recurring issue with model results for these waters, as reported in detail by Myksvoll et al. (2018). In the Barents Sea the salinity biases vary from region to region, while the bias in the

upper Norwegian Sea deep basin have values in the range $-0.3 - -0.1$.

The temperature bias is low (mostly within $\pm 0.3\,^{\circ}$C) in the coastal regions and in the

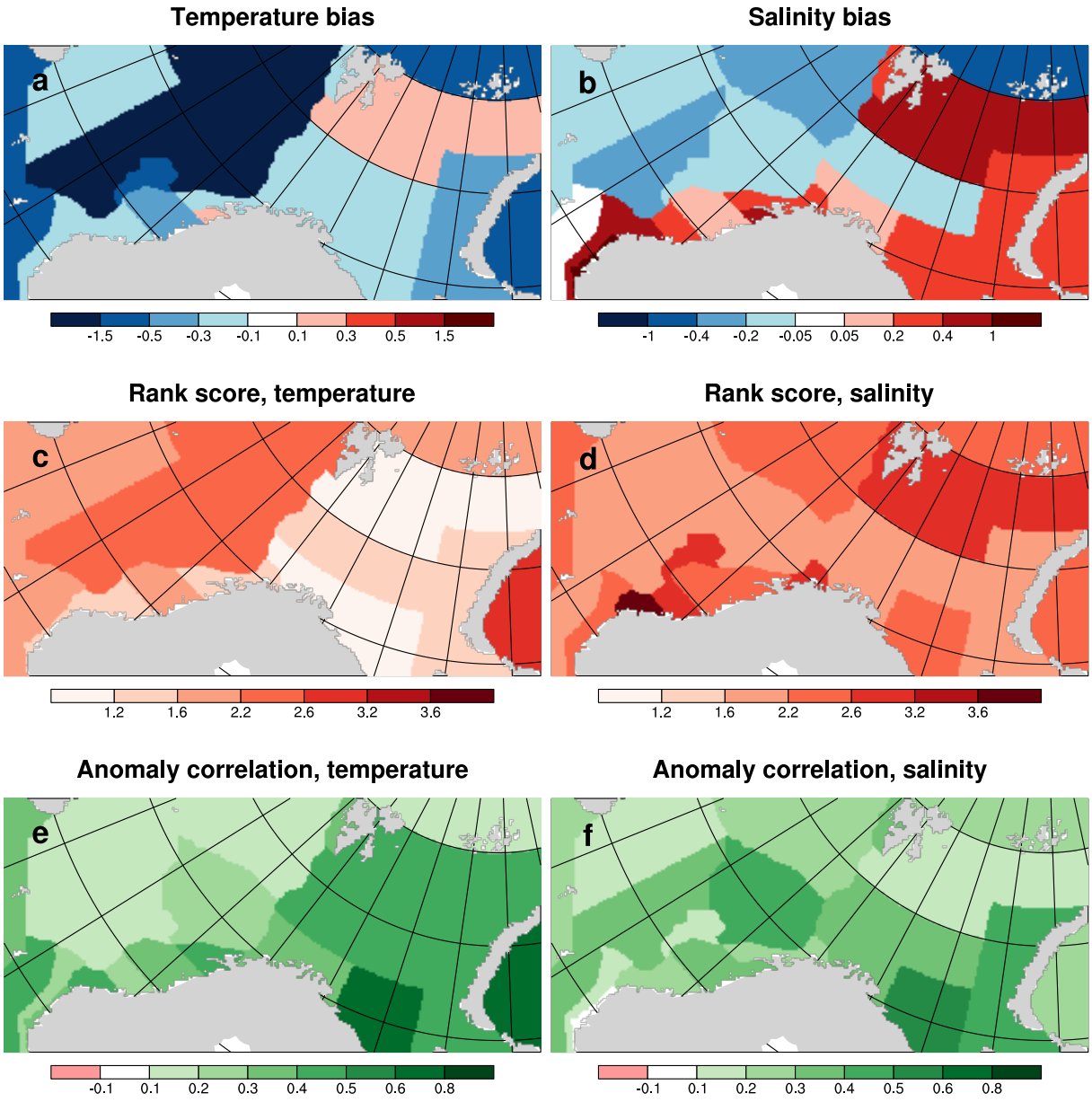

Fig. S4. Validation statistics for temperature and salinity, for data from the depth range 0-100 m available from WOD for all four simulation years, and the corresponding model results. Results have been aggregated in the analysis regions that are displayed in Fig. S1. All results represent averages where data from each of the four years are given the same weight (0.25). Additional details and a discussion of these results are provided in the text.

Barents Sea. However, in the upper 100 m of the Norwegian Sea deep basin the model results exhibit a strong negative bias of about -2 °C.

Next, we define a rank score which is constructed in order to provide information of how well the model results capture the spatio-temporal variability of temperature and salinity in the upper 100 m. This is achieved by first introducing a pseudo bias defined as

$$pBIAS(r, y, \hat{y}) = \frac{1}{N(r, y)} \sum_{n=1}^{N(r,y)} [x_n^m(\hat{y}) - x_n^o(y)] \tag{S5}$$

where $x^m(\hat{y})$ is the model result at the time and day of the observation, but extracting the result from simulation year $\hat{y}$. Here we consider results from four simulation years. Hence, for each region r there are four $pBIAS$ values for each year y. So e.g. using observations for region 1 from 1966 gives rise to four pseudo bias values: $pBIAS(1, 1966, 1966)$, $pBIAS(1, 1966, 1980)$, $pBIAS(1, 1966, 1992)$ and $pBIAS(1, 1966, 2006)$. Hence, $pBIAS(r, y, y) = BIAS(r, y)$.

The absolute values of the four $pBIAS$ values are sorted by magnitude (lowest to highest), and the position, or rank, of $pBIAS(r, y, y)$ is identified. Then, for each region and each we have four rank values (one for each of the four years). The averaged rank values are thus from the discrete set of $\{1, 1.25, 1.5, \ldots, 3.5, 3.75, 4\}$. The resulting ranks are displayed in Fig. S4c,d.

The best representation of spatio-temporal variability occurs when the smallest bias values are associated with matching the observation years with the same simulation year, i.e. a rank of 1. If there is no relation between the temporal variability in observations and model results, the expected rank is 2.5. We find that with one exception the simulation results for spatio-temporal temperature variability have values ≤ 1.5 in all regions along the Norwegian coast and in the Barents Sea. This variability is however

not captured well in the deep basin regions of the Norwegian Sea. The spatio-temporal variability of salinity is generally not reproduced with any quality in the simulations.

We introduce offset from monthly climatology values x^c as $d^{m,o} = x^{m,o} - x^c$. Following Murphy & Epstein (1989) the anomaly correlation coefficient ACC is then given by

$$ACC(r,y) = \frac{\sum_{n=1}^{N(r,y)}[(d^m(n) - \overline{d^m})(d^o(n) - \overline{d^o})]}{N(r,y)s_{d^m}s_{d^o}} \tag{S6}$$

where overbars denote average values, and s_d is the standard deviation of property d. Monthly climatologies were derived from the $0.25°$ resolution ARMOR3d product (Guinehut et al. 2012) which is based on in situ and remote sensing observations. Climatologies were computed from results for the period 1993 – 2016, and interpolated onto the

Table S1. Results from validation vs. World Ocean Database temperatures for a selection of regions (see Fig. S1 for definitions of the various region no.s). Computations are based on observations and model results from the R4 configuration for the period April – August (inclusive). Statistics for each calendar month are given the same weight. Definitions for bias and anomaly correlation coefficient (ACC) are given by equations S4 and S6, respectively.

	Region no.							
	4	5	6	7	8	9	10	12
BIAS, temperature								
1966	-0.1	-0.1	0.2	0.9	-0.0	-0.4	-0.2	-0.2
1980	-0.2	-0.3	-0.4	-0.1	0.1	-0.1	-0.5	-0.4
1992	-0.1	-0.2	-0.5	-0.1	-0.2	-0.0	-0.1	0.2
2006	-0.6	-0.3	-0.7	0.8	-0.2	-0.1	-0.2	0.1
average	**-0.3**	**-0.2**	**-0.4**	**0.4**	**-0.1**	**-0.1**	**-0.2**	**-0.1**
ACC, temperature								
1966	0.6	0.3	0.5	0.5	0.6	0.2	0.3	0.4
1980	0.4	0.4	0.2	0.2	0.5	0.3	0.1	0.3
1992	0.4	0.4	0.5	0.5	0.2	0.2	0.4	0.4
2006	-0.2	-0.3	0.0	0.5	0.2	-0.1	0.2	0.5
average	**0.3**	**0.2**	**0.3**	**0.4**	**0.4**	**0.2**	**0.3**	**0.4**

model grid on which results for d^m are available.

The anomaly correlation coefficient results, averaged over the four simulation years, are displayed in Fig. S4e,f. We note that the anomaly correlation coefficients are positive in all analysis regions for both temperature and salinity. For temperature, the values are mostly in the range $0.2 - 0.5$ in the coastal regions and the Barents Sea regions, and lower in the Norwegian Sea deep basin. Coefficients for salinity are of similar magnitude, but without any obvious contrast between coastal, Barents Sea, and deep basin regions.

Next, further information about the quality of model results for the upper 100 m temperature for the various simulation years are given in Table S1. Here, results are given for the regions with highest concentrations of tracers and floats in the R4 configuration

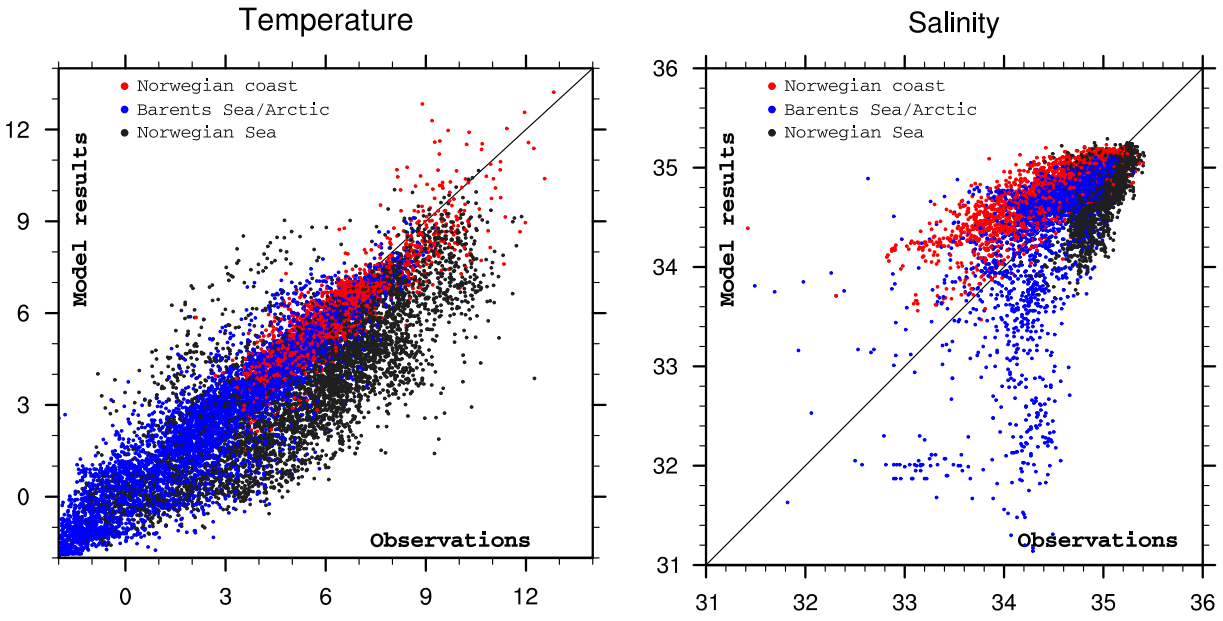

Fig. S5. Scatter diagrams for temperature and salinity, for data from the depth range 0-100 m available from WOD for all four simulation years, and the corresponding model results. The colors indicate which ocean region each observation is from. These ocean regions are compiled as follows: “Norwegian coast” (red) is analysis regions 4-9 as shown on Fig. S1; “Barents Sea/Arctic” (blue) is analysis regions 10-17; “Norwegian Sea” (black) is analysis regions 18-22. Note that the observation/model match-ups were drawn in random order, in order not to discriminate any colored region to the others due to overlapping dots.

(as shown by the distribution results in section 3). We find that the variations in the results from year to year are moderate. Nevertheless, we note that the temperature ACC results for regions 4 (*Møre coast*) and 5 (*Trønderlag coast*) are negative during 2006. This will be relevant when interpreting 2006 temperature results along tracer advection pathways and float trajectories from seeding region *Møre*.

Finally, a set of scatter diagrams are provided as Fig. S5. Color coding has been adopted in order to shed light on the contrasting results for the three sets of analysis regions for which validation results were discussed above. The scatter plots provides an additional illustration to the bias results in Fig. S4a,b: model results have a cold bias in the Norwegian Sea and much smaller differences to temperature observations elsewhere. The model salinity is higher than observations in the coastal regions, and lower in the Norwegian Sea. In the Barents Sea and Arctic region, the validation results for salinity is more mixed.

S5. Drift variability with configuration R4

Here we present a set of depictions of 61 day simulated drift from the three spawning regions in the R4 configuration. Shown on the next three pages by thin blue lines are the 61 days trajectories of the online Lagrangian floats that were seeded on 1 April 00 UTC. The end position of the trajectories after the 61 day drift (1 June 00 UTC) is displayed by black dots. This is obviously only a very small subset of the full results, as we display trajectories from only one of a total of 732 seeding times.

From Fig. S6, S7, and S8, we note that the interannual variability of drift pathways is strong. Inspecting the results for seeding region *Møre* (Fig. S6) we note that the the trajectories are displaced further offcoast in 1966 than in the other three years. For trajectories emanating from seeding region *Yttersida* (Fig. S7) we find contrasting results between years for drift along the continental slope and into the Barents Sea. For seeding region *Vestfjorden* (Fig. S8) we observe that the degree of retention inside Vestfjorden changes between years, and impacts how far downstream the Lagrangian floats are advected by the 61 day drift that is displayed.

The trajectories are displayed on top of filled grey contour shades that display the region were 90% of the Eulerian tracer mass that was introduced at the same time, is found after 61 days. Note that the tracer mass is not evenly distributed in the grey shaded regions. We stress that while trajectories display a history of 61 day drift, the Eulerian tracer fields are snapshots only, and hence that the situations displayed are impacted by the synoptic weather situation in the final days leading up to 1 June.

Statistics and integrated results for the full sets of seeded Lagrangian floats are given in the main manuscript.

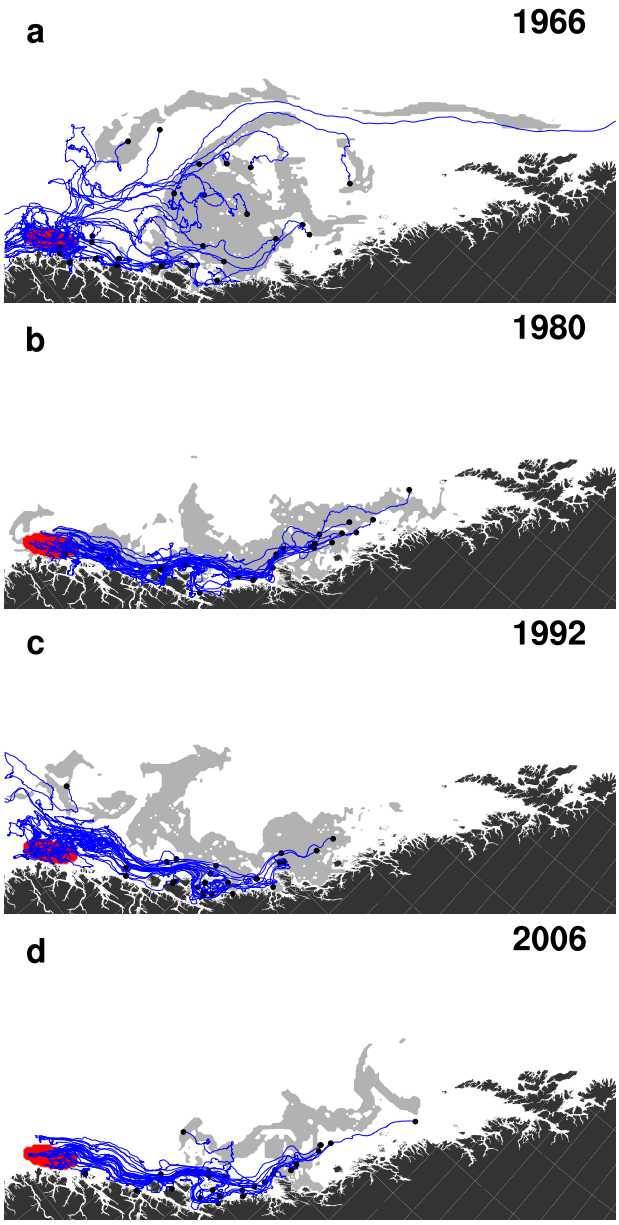

Fig. S6. Sample trajectories from seeding region *Møre*, for Lagrangian floats that were seeded on 1 April 00 UTC. Positions after 61 days' drift are shown by black dots. The region to which the Eulerian tracer has been advected and diffused at the same time (1 June 00 UTC) is displayed as a grey shaded region. The seeding region is displayed in red. Panels a,b,c,d gives results for 1966, 1980, 1992 and 2006, respectively (years are also displayed to the top left). See the text for details.

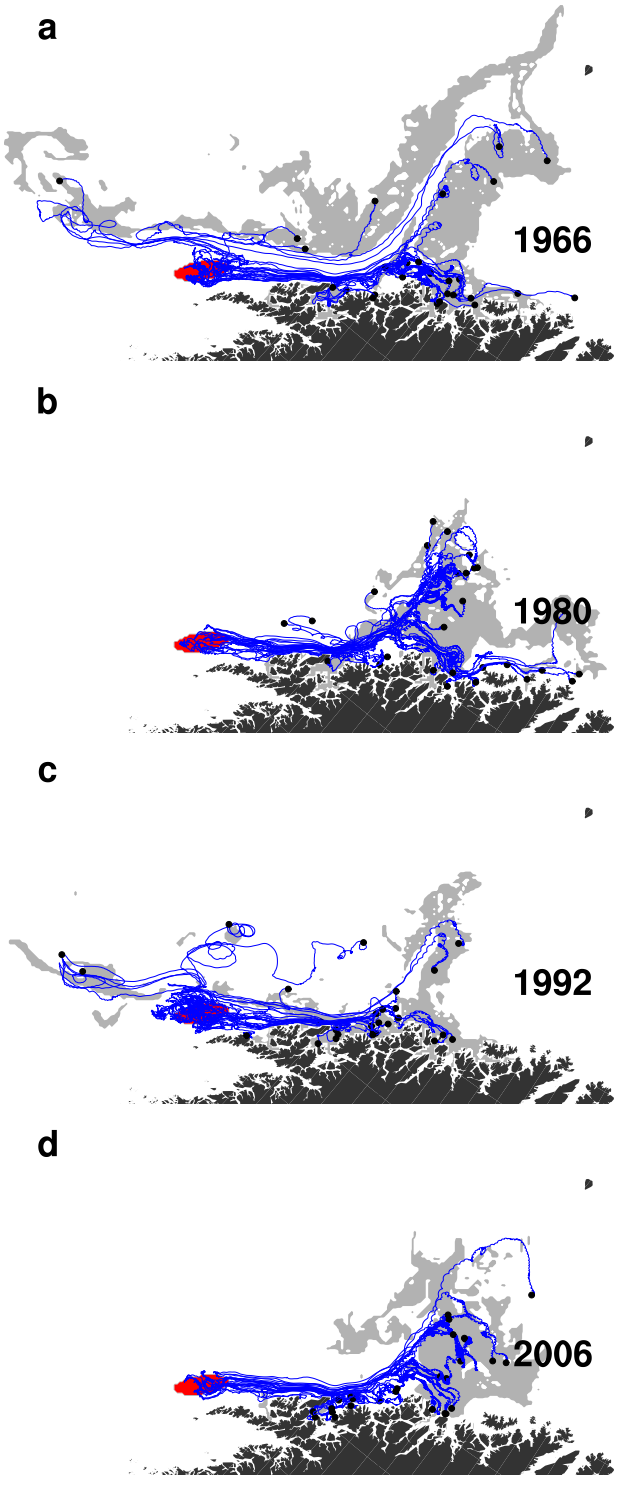

Fig. S7. As Figure S6, but for seeding region *Yttersida*.

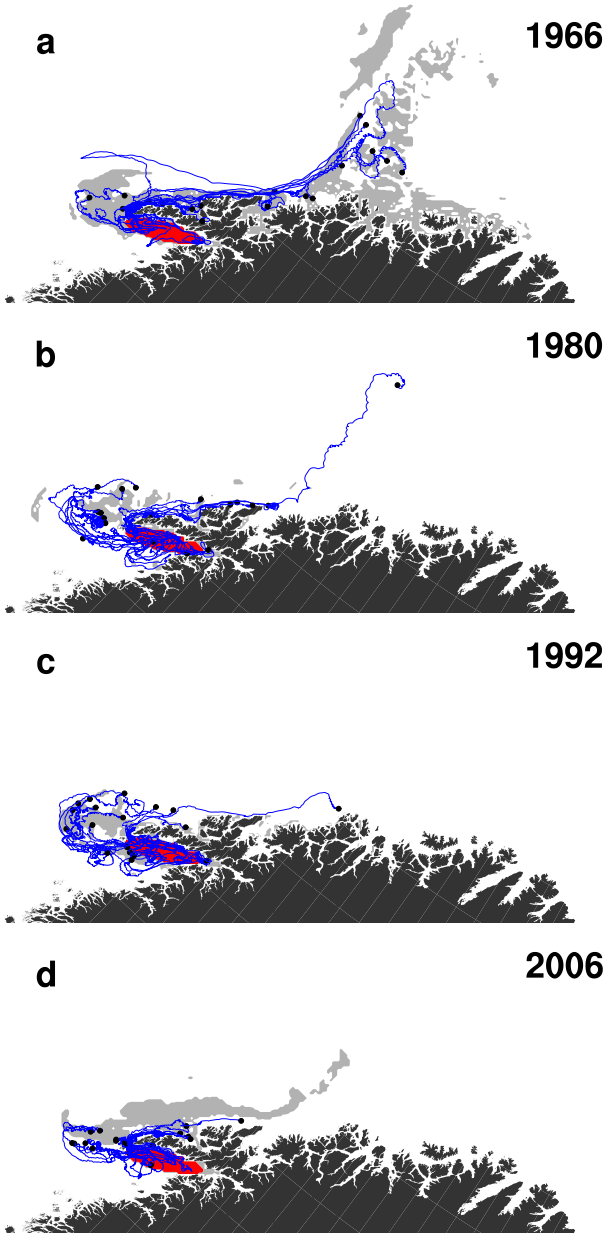

Fig. S8. As Figure S6, but for seeding region *Vestfjorden*.

LITERATURE CITED

Boyer TP, Antonov JI, Baranova OK, Coleman C, Garcia HE, Grodsky A, Johnson DR, Locarnini RA, Mishonov AV, O'Brien TD, Paver CR, Reagan JR, Seidov D, Smolyar IV, Zweng MM (2013) World Ocean Database 2013. In: Levitus S, Mishonov A (eds) NOAA Atlas NESDIS 72:209pp doi:10.7289/V5NZ85MT

Fick A (1855) Über diffusion. (In German.) Ann Phys Chem 170: 59–86 doi:10.1002/andp.18551700105

Guinehut S, Dhomps AL, Larnicol G, Le Traon PY (2012) High resolution 3-D temperature and salinity fields derived from in situ and satellite observations. Ocean Sci 8:845-857 doi:10.5194/os-8-845-2012

Jakobsen PK, Ribergaard MH, Quadfasel D, Schmith T, Hughes CW (2003) Near-surface circulation in the northern North Atlantic as inferred from Lagrangian drifters: Variability from the mesoscale to interannual. J Geophys Res 108:3251 doi:10.1029/2002JC001554

Murphy AH, Epstein ES (1989) Skill scores and correlation coefficients in model verification. Mon Weather Rev 117:572–581 doi:10.1175/1520-0493(1989)117<0572:SSACCI>2.0.CO;2

Myksvoll MS, Sandvik AD, Albretsen J, Asplin L, Johnsen IA, Karlsen Ø, Kristensen NM, Melsom A, Skardhamar J, Ådlandsvik B (2018) Evaluation of a national operational salmon lice monitoring system – From physics to fish. PLOS ONE 13:e0201338 doi:10.1371/journal.pone.0201338